A GPI processing phospholipase A2, PGAP6, modulates Nodal signaling in embryos by shedding CRIPTO

Gun-Hee Lee,[1,2]* Morihisa Fujita,[4]* Katsuyoshi Takaoka,[3] Yoshiko Murakami,[1,2] Yoshitaka Fujihara,[1,2] Noriyuki Kanzawa,[1,2] Kei-ichi Murakami,[1,2] Eriko Kajikawa,[5] Yoko Takada,[1,2] Kazunobu Saito,[1,2] Masahito Ikawa,[1,2] Hiroshi Hamada,[3,5] Yusuke Maeda,[1,2] and Taroh Kinoshita[1,2]

[1]Research Institute for Microbial Diseases, [2]World Premier International Immunology Frontier Research Center, and [3]Graduate School of Frontier Biosciences, Osaka University, Suita, Osaka 565-0871, Japan
[4]The Key Laboratory of Carbohydrate Chemistry and Biotechnology, Ministry of Education, School of Biotechnology, Jiangnan University, Wuxi, Jiangsu 214122, China
[5]Center for Developmental Biology, Institute of Physical and Chemical Research, Kobe, Hyogo 650-0047, Japan

Glycosylphosphatidylinositol-anchored proteins (GPI-APs) can be shed from the cell membrane by GPI cleavage. In this study, we report a novel GPI-processing enzyme, termed post-glycosylphosphatidylinositol attachment to proteins 6 (PGAP6), which is a GPI-specific phospholipase A2 mainly localized at the cell surface. CRIPTO, a GPI-AP, which plays critical roles in early embryonic development by acting as a Nodal coreceptor, is a highly sensitive substrate of PGAP6, whereas CRYPTIC, a close homologue of CRIPTO, is not sensitive. CRIPTO processed by PGAP6 was released as a lyso-phosphatidylinositol-bearing form, which is further cleaved by phospholipase D. CRIPTO shed by PGAP6 was active as a coreceptor in Nodal signaling, whereas cell-associated CRIPTO activity was reduced when PGAP6 was expressed. Homozygous *Pgap6* knockout mice showed defects in early embryonic development, particularly in the formation of the anterior–posterior axis, which are common features with *Cripto* knockout embryos. These results suggest PGAP6 plays a critical role in Nodal signaling modulation through CRIPTO shedding.

Introduction

Glycosylphosphatidylinositol (GPI) is a glycolipid widely used among eukaryotes as membrane anchors for many cell surface proteins (Ferguson et al., 2009). GPI is biosynthesized and transferred to proteins in the ER. After GPI attachment to proteins, remodeling of GPI moieties on GPI-anchored proteins (GPI-APs) occurs during transport (Tanaka et al., 2004; Tashima et al., 2006; Maeda et al., 2007; Fujita et al., 2009). Those remodeling reactions confer unique features on GPI-APs, including lipid raft association on the membrane (Maeda et al., 2007). Another feature of GPI-APs is their cleavage within the GPI moiety by GPI-cleaving enzymes and shedding from the membrane (Fujihara and Ikawa, 2016). The number of proven examples of GPI-cleaving enzyme–mediated GPI-AP shedding under physiological conditions is small (Fujihara and Ikawa, 2016). Theoretically, the shedding of GPI-APs has two biological modes of action: (1) shed GPI-APs act at sites remote from the original cells and affect the fate of other cells; and (2) the initiation of specific activities suppressed by inhibitory GPI-APs on the same cells (Fujihara and Ikawa, 2016). There are two examples of the latter mode; shedding of TEX101 from sperm by testis type of angiotensin-converting enzyme is involved in sperm maturation (Kondoh et al., 2005; Fujihara et al., 2013b) and shedding of a metalloprotease inhibitor RECK by glycerophosphodiester phosphodiesterase 2, resulting in metalloprotease-mediated degradation of a Notch ligand DLL1, which, in turn, reduces Notch signaling in adjacent progenitor cells to induce differentiation into neurons (Park et al., 2013). A clear example of the former mode has not been demonstrated (Fujihara and Ikawa, 2016).

During embryonic development, Nodal signaling is required for many aspects, including anterior–posterior axis patterning, mesoderm induction, and left–right axis specification (Tian and Meng, 2006; Shen, 2007). CRIPTO, a GPI-AP (Minchiotti et al., 2000), forms a complex with type I and II activin receptors for Nodal on the membrane and induces cell-autonomous signaling (Yan et al., 2002). In addition, a

*G.-H. Lee and M. Fujita contributed equally to this paper.

Correspondence to Taroh Kinoshita: tkinoshi@biken.osaka-u.ac.jp

Abbreviations used: DAF, decay-accelerating factor; ES, embryonic stem; ESI, electrospray ionization; GPI, glycosylphosphatidylinositol; GPI-AP, glycosylphosphatidylinositol-anchored protein; KO, knockout; LC, liquid chromatography; MS, mass spectrometry; MS/MS, tandem mass spectrometry; m/z, mass-to-charge ratio; PGAP, post-glycosylphosphatidylinositol attachment to proteins; PI-PLC, phosphatidylinositol-specific PLC; PLA2, phospholipase A2; PLD, phospholipase D; PM, plasma membrane; uPAR, urokinase-type plasminogen activator receptor.

The Rockefeller University Press $30.00
J. Cell Biol. Vol. 215 No. 5 705–718
https://doi.org/10.1083/jcb.201605121

biologically active, soluble form of CRIPTO is generated by GPI cleavage (Watanabe et al., 2007). The soluble form of CRI PTO is required for non–cell autonomous CRIPTO-Nodal signaling in mammalian cells (Yan et al., 2002; Parisi et al., 2003), which is critical for axial mesendoderm formation (Chu et al., 2005). However, molecular mechanisms of CRIPTO shedding have not been clarified (Minchiotti et al., 2001; Yan et al., 2002).

We previously reported that post-glycosylphosphatidylinositol attachment to proteins 3 (PGAP3) is a Golgi-resident, GPI-specific phospholipase A2 (GPI-PLA2) involved in fatty acid remodeling of GPI-APs (Fujita et al., 2006; Maeda et al., 2007). In the remodeling process, PGAP3 is required for the removal of an unsaturated fatty acid from the sn-2 position. A bioinformatics approach revealed that PGAP3, Per1p (a yeast homologue of PGAP3), and alkaline ceramidase belong to a membrane-bound hydrolase superfamily, termed CREST (alkaline ceramidase, PAQR receptor, Per1, SID-1, and TMEM8) (Pei et al., 2011). In this study, we identified an uncharacterized gene, TMEM8A, here renamed PGAP6, which has close similarity to PGAP3 in the superfamily members. Our data show that PGAP6 is a GPI-PLA2 expressed on the cell surface, sheds CRIPTO as an active Nodal coreceptor, and is critical for anterior–posterior axis formation in embryonic development through modulating CRIPTO-Nodal signaling.

Results

TMEM8A/PGAP6 is involved in GPI-AP processing at the cell surface

CREST members share seven predicted transmembrane segments containing five conserved residues (three His, Asp, and Ser). TMEM8 family proteins, which are located near the PGAP3 gene cluster, are conserved in vertebrates and include three members (TMEM8A, B, and C) in mammals (Pei et al., 2011). Among them, TMEM8A has conserved putative catalytic amino acids within transmembrane domains at the C-terminal regions (Fig. 1 A). In addition, TMEM8A has an unannotated N-terminal region and an EGF-like domain after the signal sequence for ER insertion. TMEM8A was detected by anti-TMEM8A mAb on human embryonic carcinoma NTE RA2 cells and HEK293T cells by flow cytometry, indicating that TMEM8A, unlike Golgi-resident PGAP3, is expressed on the cell surface (Fig. 1 B). To further characterize TMEM8A, TMEM8A or HA-tagged TMEM8A (HA-TMEM8A) was expressed in CHO 3B2A cells. Nontagged TMEM8A was detected on the cell surface (Fig. 1 C). HA-TMEM8A was also detected on the cell surface (Fig. 1 D) and appeared in 120- and 90-kD bands (Fig. 1 E, lane NT). The 120-kD band was sensitive to PNGase and resistant to EndoH, indicating that it represents a mature cell surface TMEM8A protein (Fig. 1 E, lanes EnH and PNG). The 90-kD band was sensitive to both PNGase and EndoH, indicating that it has immature *N*-glycans. Subcellular fractionation and microscopic observation confirmed that the 120-kD protein is localized in the plasma membrane (PM) and that the 90-kD protein is localized in the ER (Fig. 1, F and G). The ER form might be an intermediate during transport.

We tested whether TMEM8A is involved in GPI-AP processing using CHO 3B2A cells overexpressing HA-TMEM8A. TMEM8A significantly reduced amounts of two GPI-APs, CD59 and decay-accelerating factor (DAF), whereas another GPI-AP urokinase-type plasminogen activator receptor (uPAR) was only slightly decreased (Fig. 2 A). Because TMEM8A has similarity to PGAP3 and decreased the levels of GPI-APs, we renamed it PGAP6 (for post-GPI attachment to proteins 6) as a protein involved in the processing of GPI-APs.

Because different GPI-APs showed different sensitivity to PGAP6, we searched for a sensitive substrate GPI-AP, especially among those known to be released from the cell surface, and found CRIPTO is highly sensitive (Fig. 2 B). Strikingly, CRYPTIC, another GPI-AP and a close homologue of CRIPTO, was not decreased from the cell surface even with overexpression of PGAP6 (Fig. 2 B), indicating that PGAP6 has specificity and selectivity against substrate GPI-APs.

We next addressed the molecular mechanisms of decreased GPI-APs on the cell surface. CRIPTO exists in soluble and membrane-bound forms (Yan et al., 2002; Watanabe et al., 2007). Because CRIPTO was constantly released into the medium when CRIPTO-transfected HEK293T cells were cultured in the presence of 10% FCS, we analyzed the effect of PGAP6 using serum-free medium. Western blotting revealed 23- and 21-kD bands of HA-CRIPTO (Fig. 2 C). The 23-kD band represents a mature protein bearing a complex type *N*-glycan, whereas the 21-kD band represents the immature, ER form of HA-CRIPTO bearing EndoH-sensitive *N*-glycan (Fig. S1). When PGAP6 was overexpressed, the mature form of CRIPTO was nearly completely lost, whereas the ER form of CRIPTO remained (Fig. 2 C, left, top panel). The surface expression of CRIPTO was strongly reduced by PGAP6 overexpression (Fig. 2 C, top right) and secretion of HA-CRIPTO was enhanced (Fig. 2 C, left, bottom panel).

NTERA2 cells express both CRIPTO and PGAP6 (Fig. 2 D, top). CRIPTO was released from NTERA2 cells into medium (Fig. 2 D, bottom left, lane siCon), and knockdown of PGAP6 almost completely inhibited the release (lane siPGAP6), indicating that endogenous PGAP6 released endogenous CRIPTO from the cell surface. After knockdown of PGAP6, the surface expression of endogenous CRIPTO increased by ∼40% (Fig. 2 D, top and bottom right, histogram and quantified data, respectively).

Knockdown of PGAP6 in HEK293T cells also greatly decreased the release of HA-CRIPTO into the medium (Fig. 2 E, bottom left and right, Western and quantified data, respectively). After knockdown of PGAP6, the surface expression of HA-CRIPTO increased by ∼50% (Fig. S1 B). Specificity of PGAP6 knockdown was confirmed by rescue of CRIPTO release by siRNA-resistant PGAP6 but not by siRNA-resistant catalytic-dead PGAP6 (D610A; Fig. S1 C). The secretion of HA-CRIPTO was also inhibited by PGAP6 knockdown even in medium containing 10% FCS (Fig. S1 D), suggesting that the effect of serum on CRIPTO release might be dependent on PGAP6 activity. We next analyzed whether amino acid residues of PGAP6 conserved in the CREST family are required for the release of GPI-APs. All of the point mutants except the S584A mutant lost CRIPTO-releasing activity (Fig. S2), suggesting that the conserved amino acids are important for PGAP6 enzymatic activity.

PGAP6 has GPI-PLA2 activity

To determine whether PGAP6 is GPI-PLA2 as expected from similarity to PGAP3, we used partitioning with Triton X-114. Because conditions of mass spectrometry (MS) analysis of the C-terminal peptides bearing lipid-containing GPI have not been established, Triton X-114 partitioning is useful to analyze

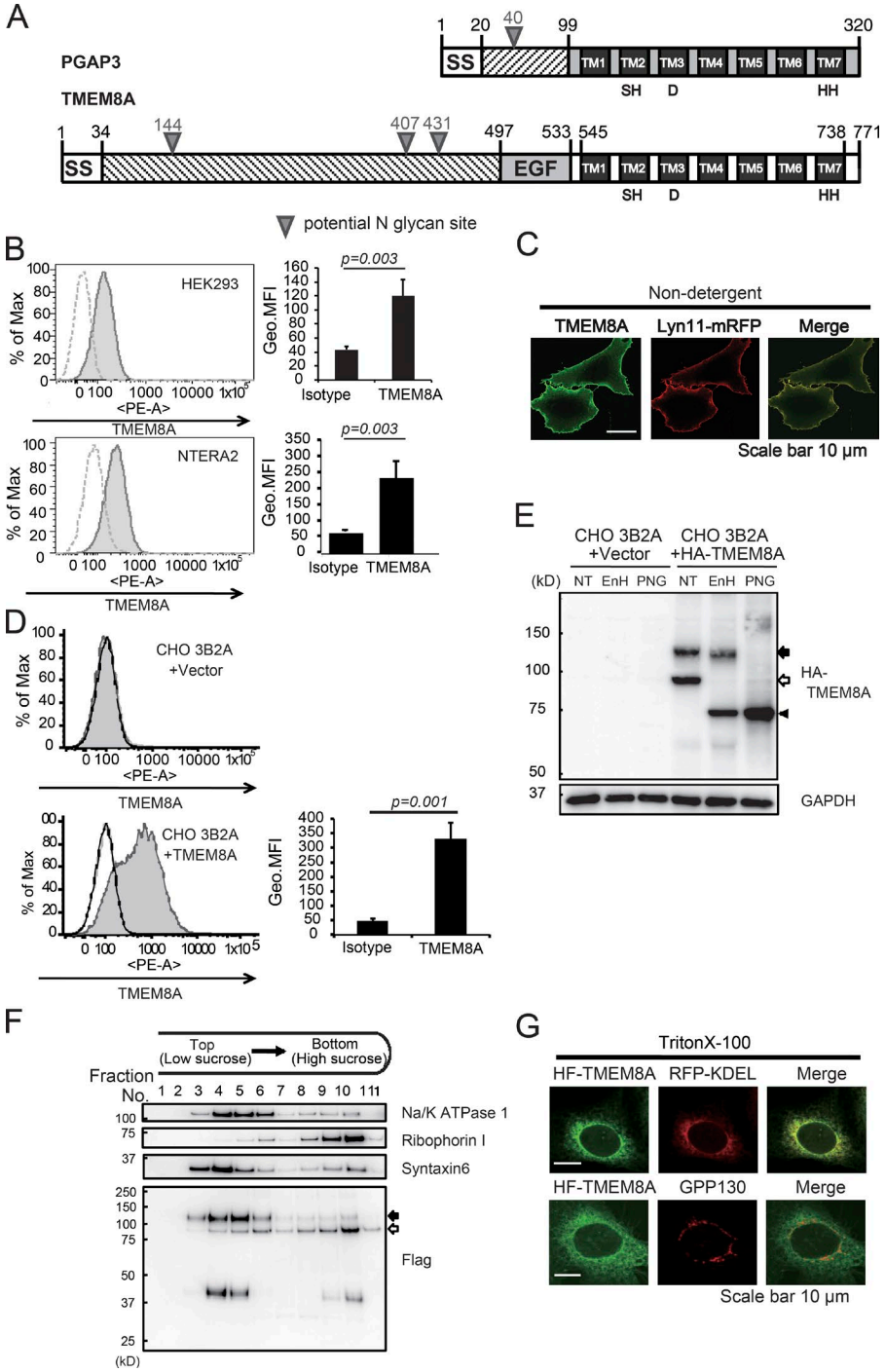

Figure 1. **TMEM8A, a homologue of PGAP3, is expressed on the cell surface.** (A) Comparison of human PGAP3 and TMEM8A proteins. Conserved residues within transmembrane regions TM2, TM3, and TM7 are indicated. Amino acid numbers are above the models. (B) Flow cytometric analysis of endogenous TMEM8A on HEK293T (top) and NTERA2 (bottom) cells. Shaded, anti-TMEM8A; dashed lines, isotype controls. Geometric means of mean fluorescence intensity (geo.MFI) and SD of three independent measurements and p-values (Student's *t* test) are shown on the right. (C) Immunofluorescence visualization of cells-surface TMEM8A. 3B2A cells expressing TMEM8A and Lyn11-mRFP (PM marker) were fixed and stained with anti-TMEM8A. (D) Flow cytometric analysis of HA-TMEM8A on CHO 3B2A cells. Cells transfected with vector (top) or HA-TMEM8A (bottom) were stained with anti-HA. Shaded, anti-HA; solid lines, isotype controls. For HA-TMEM8A–transfected cells, geo.MFI with SD of three independent measurements and p-value (Student's *t* test) is shown on the right. (E) Glycosylation of TMEM8A. Lysates of cells expressing HA-TMEM8A were treated with buffer (NT), Endo H (EnH), or PNGase F (PNG) and analyzed by Western blotting. GAPDH, loading controls. Closed arrow, 120-kD form with complex *N*-glycan; open arrow, 90-kD form with EnH-sensitive *N*-glycan; arrowhead, a deglycosylated form. (F) Subcellular fractionation of TMEM8A. Lysates of cells expressing His-Flag–tagged TMEM8A (HF-TMEM8A) were fractionated by sucrose-gradient centrifugation and Western blotted. Organelle markers: Na/K ATPase 1, PM; ribophorin I, ER; syntaxin 6, Golgi. Closed and open arrows, mature PM form and immature ER form of HF-TMEM8A, respectively. A band at 40 kD is likely degraded HF-TMEM8A. Representative data of two independent experiments. (G) Immunofluorescence visualization of an ER form of TMEM8A. 3B2A cells expressing HF-TMEM8A and RFP-KDEL (ER marker) or GPP130 (Golgi marker) were fixed and stained with anti-Flag after permeabilization with Triton X-100.

whether GPI-APs possess lipid moieties. Most CRIPTO released by PGAP6 was partitioned into the aqueous phase, and only a small amount was partitioned into the detergent phase, suggesting released GPI-APs did not have a lipid chain (Fig. S3 A). We then used His-Flag-GST-Flag–tagged CD59 (HF-GF-CD59) to determine the structure of the GPI moiety in released GPI-APs. HFGF-CD59 was released by overexpression of PGAP6 (Fig. S3 B, right). The GPI structures of released HFGF-CD59 were analyzed by MS. Four peaks containing a C-terminal peptide bearing GPI moiety were detected. In the second MS, all four peaks gave characteristic fragments derived from a GPI anchor, such as mass-to-charge ratio (m/z) 447^{+} and 609^{+}. Based on the profile of the fragment ions, we concluded that the C-terminal peptide of the parent mass (m/z $1{,}226.44^{2+}$) had a GPI glycan core structure without a phospholipid (Fig. 3 A). Three other peaks contained the same GPI core structure and a side chain linked to the first mannose with different sugar extensions known to occur in mammalian GPIs (Paulick and Bertozzi, 2008; Fig. S3 C). All four peaks were generated by hydrolysis between inositol and phosphate. Therefore, the released HFGF-CD59 was the product of phospholipase D (PLD)–mediated cleavage.

These results suggest that if PGAP6 is a GPI-PLA2, lyso–GPI-AP generated by PGAP6 is subsequently cleaved by PLD. We next assessed this scenario by determining the number of fatty chains linked to GPI-APs in cells overexpressing PGAP6.

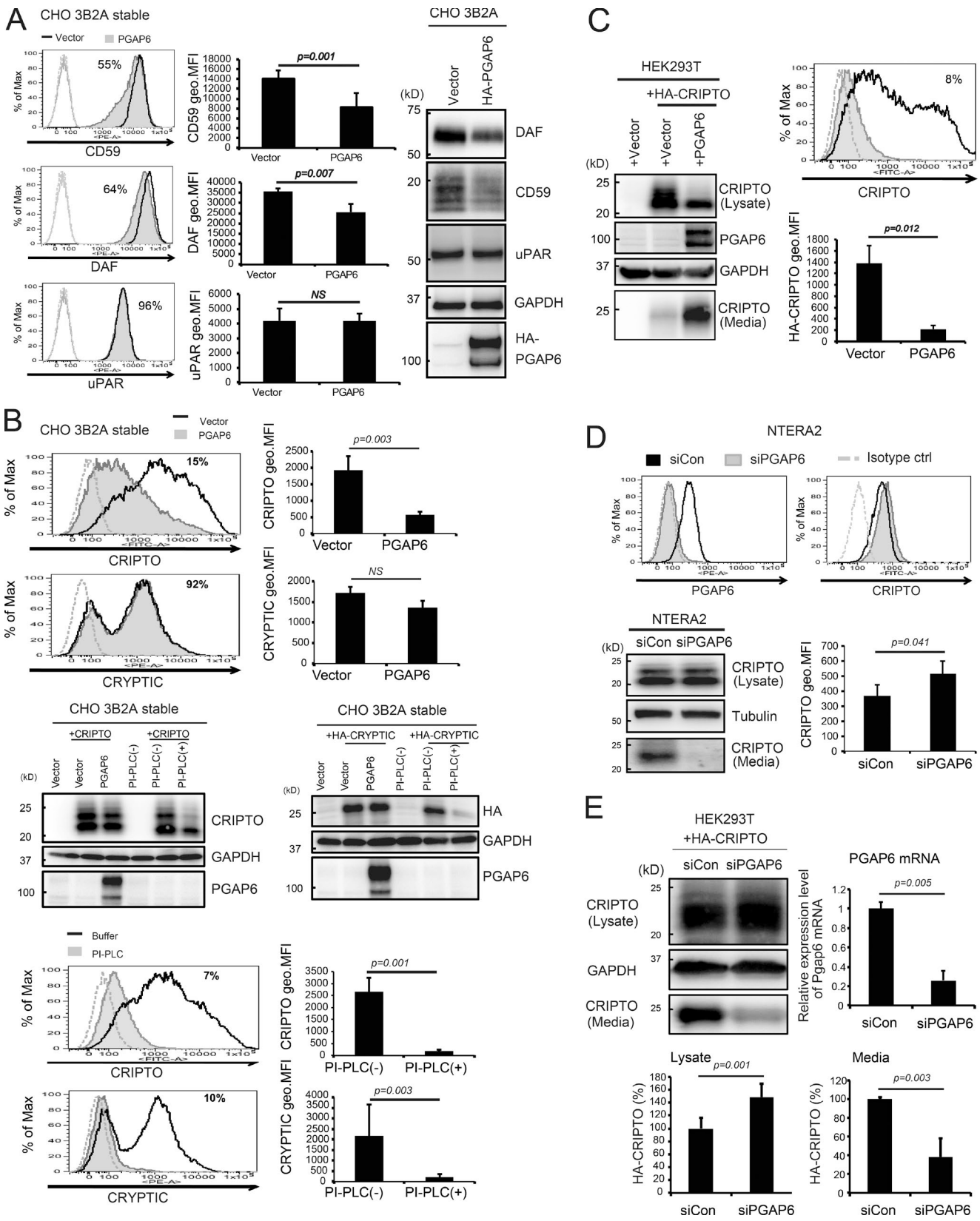

Figure 2. **TMEM8A is involved in GPI-AP processing.** (A) TMEM8A/PGAP6 overexpression selectively decreased some GPI-APs. Right: Western blotting of 3B2A cells stably transfected with vector or HA-PGAP6. Left: flow cytometry of the same cells. Black lines, vector-transfected cells; shaded areas, cells expressing HA-PGAP6; gray lines, vector-transfected cells stained with second antibody only; gray dashed lines, HA-PGAP6–transfected cells stained with second antibody only. PGAP6 decreased CD59 to 55%, DAF to 64%, and uPAR to 96% of wild-type levels. Geometric means of mean fluorescence intensity (geo.MFI) with SD of three independent measurements and p-values (Student's *t* test) are shown to the right of each histogram. (B) CRIPTO is very sensitive, whereas CRYPTIC is resistant to PGAP6. CHO 3B2A cells stably expressing CRIPTO or HA-tagged CRYPTIC were transfected with PGAP6 or a vector.

For this, we used hydrophobic chromatography with octyl-Sepharose. The reporter GPI-AP VSVGts-FF-mEGFP-GPI consists of the extracellular domain of temperature-sensitive vesicular stomatitis virus G protein, a furin cleavage site, a Flag tag, modified EGFP, and a GPI attachment signal (Tashima et al., 2006). Upon arrival at the trans-Golgi network, the reporter becomes a smaller molecule termed Flag-mEGFP-GPI by furin cleavage. Sufficient amounts of Flag-mEGFP-GPI were isolated from PGAP6-overexpressed cell lysates for chromatographic analysis. Flag-mEGFP-GPI harboring two fatty chains isolated from wild-type cells was eluted in fractions 15 and 16 (Fig. 3 B, a), whereas Flag-mEGFP-GPI from PGAP6-overexpressing cells was eluted in fractions 13 and 14, one fraction earlier than the wild-type protein (Fig. 3 B, b). This suggested that one fatty acid was removed by PGAP6. To confirm this, Flag-mEGFP-GPI from wild-type cells was treated with honeybee PLA2 and subjected to the same column either alone or after mixing with Flag-mEGFP-GPI from PGAP6-overexpressing cells. As shown in Fig. 3 B (c and b + c), they were coeluted. These results suggest that PGAP6 has GPI-PLA2 activity.

We next analyzed whether GPI-PLD (GPLD1) is involved in the PGAP6-dependent release process. We analyzed GPLD1-knockout (KO) HEK293 cells in serum-free medium to eliminate the effects of GPI-PLD in the serum. Flow cytometric analysis showed the surface expression of CRIPTO in GPLD1-KO expressing PGAP6 was reduced similar to that in wild-type cells expressing PGAP6 (Fig. 3 C). Therefore, GPI-PLD was not required for PGAP6-dependent CRIPTO release itself. However, a significant fraction of CRIPTO released by PGAP6 in the absence of GPI-PLD was partitioned to the detergent phase (Fig. 3 D, right, middle panel), indicating that CRI PTO bearing lyso-GPI released from the cell membrane is eventually converted to the lipid-free form by the action of GPI-PLD or other PLD active on lyso-GPI (Fig. 4 A).

Shedding of CRIPTO by PGAP6 modulates Nodal signaling: Shed CRIPTO acted on other cells as a Nodal coreceptor, whereas cell-associated CRIPTO activity was decreased by coexpression of PGAP6

CRIPTO functions as an essential coreceptor of a heteromeric receptor for TGF-β ligands, including Nodal (Shen and Schier, 2000; de Castro et al., 2010). CRIPTO could act as a Nodal coreceptor in two ways, either in cis or in trans. We first analyzed the effects on the trans functions of CRIPTO. CRI PTO-expressing HEK293 cells were cultured, and activity of CRIPTO released into the culture media was assessed by incubating the culture media with responder cells expressing Nodal receptor and (n2)7-luciferase reporter (Saijoh et al., 2000). CRIPTO released in the absence of exogenous PGAP6 showed Nodal signaling activity in trans, which was enhanced by the expression of PGAP6 (Fig. 5 A). In contrast, culture medium collected from PGAP6 knockdown cells did not activate Nodal signaling in trans (Fig. 5 B). Endogenous CRIPTO released from NTERA2 cells also had trans Nodal coreceptor activity, which was inhibited by knockdown of PGAP6 (Fig. 5 C). These results indicate that CRIPTO released by PGAP6 has an ability to function as a Nodal coreceptor on other cells.

Because PGAP6 expression reduced cell surface CRIPTO, we investigated whether cis Nodal signaling was affected by PGAP6. There was a 2.5-fold increase in reporter response with HA-CRIPTO expression. This increased response was decreased by cotransfection of PGAP6 with HA-CRIPTO (Fig. 5 D), although this inhibition was not complete, probably because of the trans activity of secreted HA-CRIPTO. Moreover, HA-CRIPTO induced the phosphorylation of Smad2 in HEK293T cells, and this phosphorylation was impaired in cells cotransfected with PGAP6 (Fig. 5 E). These results indicate that PGAP6 modulates both cis and trans CRIPTO-dependent Nodal signaling through cleavage of the GPI anchor of CRIPTO.

CRIPTO shedding by PGAP6 is inhibited by mutations in *PGAP1* and *PIGN*

It was reported that two recessive mutations in GPI biosynthetic genes *Pign* and *Pgap1* in mice caused defective Cripto signaling and holoprosencephaly, a form of impaired development of the forebrain (McKean and Niswander, 2012). PIGN (Pign in mice) is required for the addition of an ethanolamine phosphate side chain to the first mannose on GPI during biosynthesis in the ER (Hong et al., 1999), and PGAP1 (Pgap1 in mice) acts as a GPI-inositol deacylase after GPI transfer to proteins (Tanaka et al., 2004; Fig. 4). These observations prompted us to analyze whether PGAP6 processes and releases CRIPTO in the *PIGN* and *PGAP1* mutant backgrounds. CRIPTO transfected into *PGAP1* mutant cells was expressed on the cell surface at levels substantially lower than those on wild-type cells (Fig. 6 A). The slow transport of CRIPTO from the ER might explain the observed phenotypes (Tanaka et al., 2004). When PGAP6 was cotransfected with CRIPTO, the expression of CRIPTO on the surface of *PGAP1* mutant CHO C10 cells was only slightly decreased (statistically not significant), whereas CRIPTO on parental CHO 3B2A cells was reduced significantly (Fig. 6 A). Western blotting also showed that CRIPTO was not released into the culture medium in *PGAP1* mutant cells expressing PGAP6 (Fig. 6 B, bottom). The lipid properties of GPI-APs in *PGAP1* mutant cells were then analyzed by octyl-Sepharose chromatography

(top and bottom) Flow cytometry. The cell surface levels of CRYPTIC as assessed by anti-HA staining and FACS were similar with and without PGAP6 overexpression, whereas CRIPTO levels were drastically decreased with PGAP6. Both CRIPTO and CRYPTIC were similarly sensitive to PI-PLC. Geo.MFI with SD of three independent measurements and p-values (Student's *t* test) are shown to the right of each histogram in top and bottom panels. (middle) Western blot data showing PGAP6 expression in PGAP6-transfected cells. (C) CRIPTO is shed into the culture medium by PGAP6. HEK293T cells transiently expressing HA-CRIPTO alone or with PGAP6 were cultured in serum-free medium for 6 h. The cells were lysed, and culture supernatants were immunoprecipitated by anti-HA. The cell lysates and immunoprecipitates were analyzed by Western blotting (left). GAPDH, loading controls. Flow cytometry confirmed a nearly complete loss of mature, cell-surface HA-CRIPTO by PGAP6 (top right). Black line, HA-CRIPTO alone; shaded area, HA-CRIPTO with PGAP6; gray dashed line, negative staining. Geo.MFI with SD of three independent measurements and p-value (Student's *t* test) is shown below the histogram at bottom right. (D) Knockdown of PGAP6 in NTERA2 cells inhibited the release of CRIPTO into the medium. NTERA2 cells were transfected with control RNA (siCon) or siRNA against PGAP6 (siPGAP6). NTERA2 cells were stained for PGAP6 to assess knockdown (top left) and for CRIPTO to assess changes (top right). Cell lysates and culture media were analyzed by Western blotting (bottom left). Secretion of CRIPTO into the medium was almost completely inhibited by siPGAP6 (bottom left). The cell surface CRIPTO was increased by 40% after siPGAP6 treatment ($P = 0.041$ in Student's *t* test). (E) Knockdown of PGAP6 in HEK293T cells expressing HA-CRIPTO. Knockdown efficiency was assessed at mRNA level and is shown (top right). Release of HA-CRIPTO was significantly decreased by siPGAP6 (bottom right). Quantified data are shown as the mean ± SD of three independent experiments (Student's *t* test; bottom right).

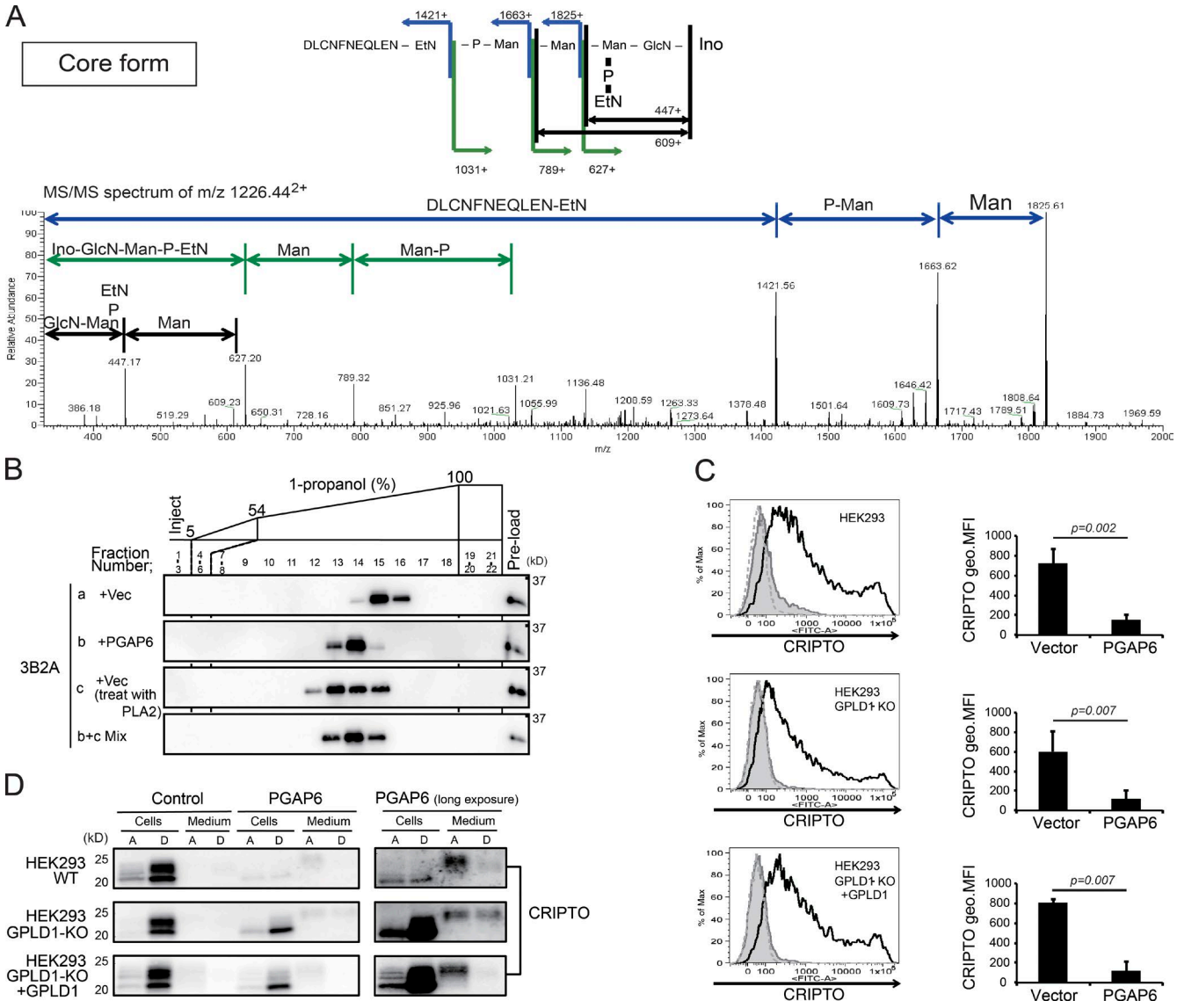

Figure 3. **Mechanisms of CRIPTO shedding.** (A) PLD-mediated GPI cleavage indicated by structural analysis of secreted GPI-AP. 3B2A cells stably expressing HFGF-CD59 were transfected with PGAP6. After 72 h, secreted HFGF-CD59 was purified from culture medium, digested in-gel by trypsin, and analyzed by LC-ESI-MS/MS. MS/MS analysis of GPI-bearing C-terminal peptide (m/z = 1,226.44^{2+}) indicated PLD-mediated cleavage of GPI. See also Fig. S3. (B) Cell-associated GPI-AP from PGAP6-expressing cells contained lyso-GPI as shown by hydrophobic chromatography. 3B2A cells stably expressing vector (a: +Vec) or PGAP6 (b: +PGAP6) were transiently transfected with VSVGts-FF-mEGFP-GPI. Flag-mEGFP-GPI purified from cell lysates was chromatographed in an Octyl-FF column with 1-propanol gradient. Fractions were analyzed by Western blotting with anti-Flag antibody. The standard lyso-form was prepared by treating Flag-mEGFP-GPI with honeybee PLA2 and analyzed alone (c: +Vec [treat with PLA2]) or after mixing with sample b (b + c Mix). (C) GPI-PLD is dispensable for CRIPTO release from the cell surface. Wild-type, GPLD1-KO, and GPLD1 rescued GPLD1-KO HEK293 cells, transiently expressing HA-CRIPTO with vector (black lines) or PGAP6 (shaded areas), were analyzed for CRIPTO by flow cytometry. Dashed lines, samples without first antibody. CRIPTO on GPLD1-KO cells was equally sensitive to PGAP6-dependent shedding. Geometric means of mean fluorescence intensity (geo.MFI) with SD of three independent measurements and p-values (Student's *t* test) are shown on the right. CRIPTO geo.MFI of wild-type, GPLD1 KO, and GPLD1-rescued GPLD1 KO cells after vector transfection were not significantly different. (D) GPI-PLD is involved in the cleavage of lyso-GPI. The same cells as shown in C were cultured in serum-free medium for 6 h. Cellular and secreted HA-CRIPTO from vector- (Control) and PGAP6-transfected (PGAP6) cells were partitioned into the aqueous (A) and detergent (D) phases after Triton X-114 solubilization. (right) Longer exposure for samples from PGAP6-transfected cells. CRIPTO secreted from PGAP6-expressing GPLD1-KO cells contained a hydrophobic fraction.

(Fig. 6 C). Flag-mEGFP-GPI proteins from *PGAP1* mutant cells were mainly eluted in fraction 16, indicating that they were more hydrophobic than those from wild-type cells because of an additional acyl chain (Fig. 3 B [a] vs. Fig. 6 C [a]). PLA2 treatment of Flag-mEGFP-GPI prepared from *PGAP1* mutant cells resulted in elution in more hydrophilic fractions (Fig. 6 C, c). Flag-mEGFP-GPI from *PGAP1* mutant cells expressing PGAP6 was eluted earlier than that from *PGAP1* mutant cells with an empty vector (Fig. 6 C, b). The eluted position was similar to that of wild type (Fig. 3 B, a), suggesting PGAP6 cleaved inositol-acylated GPI-APs to generate inositol-acylated lyso–GPI-APs. These results indicate that inositol-acylated GPI-AP is sensitive to PGAP6 but is not secreted into the medium because of the additional acyl-chain linked to inositol (Fig. 4, A and B). Consistent with a lack of CRIPTO secretion, Nodal signaling was not induced by culture media from *PGAP1* mutant cells (Fig. 6 D).

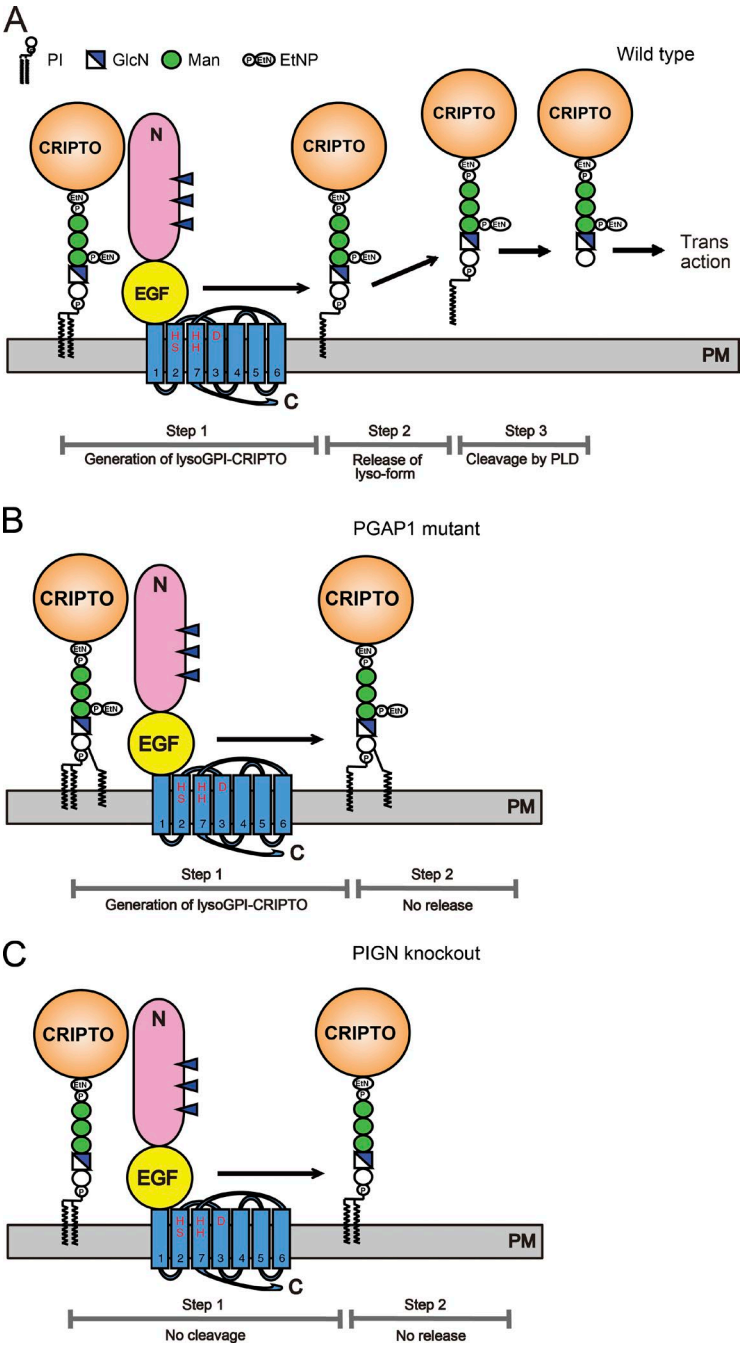

Figure 4. **Schematic of PGAP6 action on CRIPTO.** (A) Steps in the shedding of CRIPTO from PGAP6-expressing cells. (B) PGAP6 cleaves but does not shed CRIPTO from *PGAP1* mutant cells. (C) No cleavage or shedding of CRIPTO occurs in *PIGN*-KO cells.

It is known that GPI-APs, lacking a first mannose–linked ethanolamine phosphate side chain, are expressed on the *PIGN*-null cell surface, although usually at decreased levels than normal (Hong et al., 1999; Ohba et al., 2014). When CRIPTO was transfected into PIGN-KO and wild-type HEK293 cells, CRIPTO on the PIGN-KO cells, although its surface expression was slightly lower than that on wild-type cells, was resistant to PGAP6 (Fig. 6 E, bottom). Western blotting also showed that CRIPTO was not secreted into the medium by PGAP6 (Fig. 6 F), suggesting that the ethanolamine phosphate side chain was critical for cleavage by PGAP6. Culture media from PIGN-KO cells expressing CRIPTO with PGAP6 did not induce Nodal signaling (Fig. 6 G). These results indicate that mutations in *PGAP1* and *PIGN* impaired PGAP6-dependent CRIPTO secretion (Fig. 4, B and C).

Pgap6 is critical for the early embryogenesis in mouse

Cripto plays a key role in mouse embryo by acting as a Nodal coreceptor (Ding et al., 1998; Xu et al., 1999). To confirm that Pgap6 is expressed in embryo when Cripto functions, we determined *Pgap6* transcripts in day 6.2 embryos (E6.2) by in situ hybridization. *Pgap6* was weakly but widely expressed in epiblasts (Fig. 7, A and B). *Cripto* was expressed in E6.2 epiblasts, forming a gradient from high expression in the proximal region to weaker expression in the distal region (Fig. 7, E and F; Ding et al., 1998). In E6.7 embryos, *Pgap6* transcript levels decreased (Fig. 7, G and H), and in E7.7, they were below the detection limit of in situ hybridization (not depicted), suggesting that *Pgap6* is transiently coexpressed with *Cripto* in epiblasts at 6.2 d postcoitum.

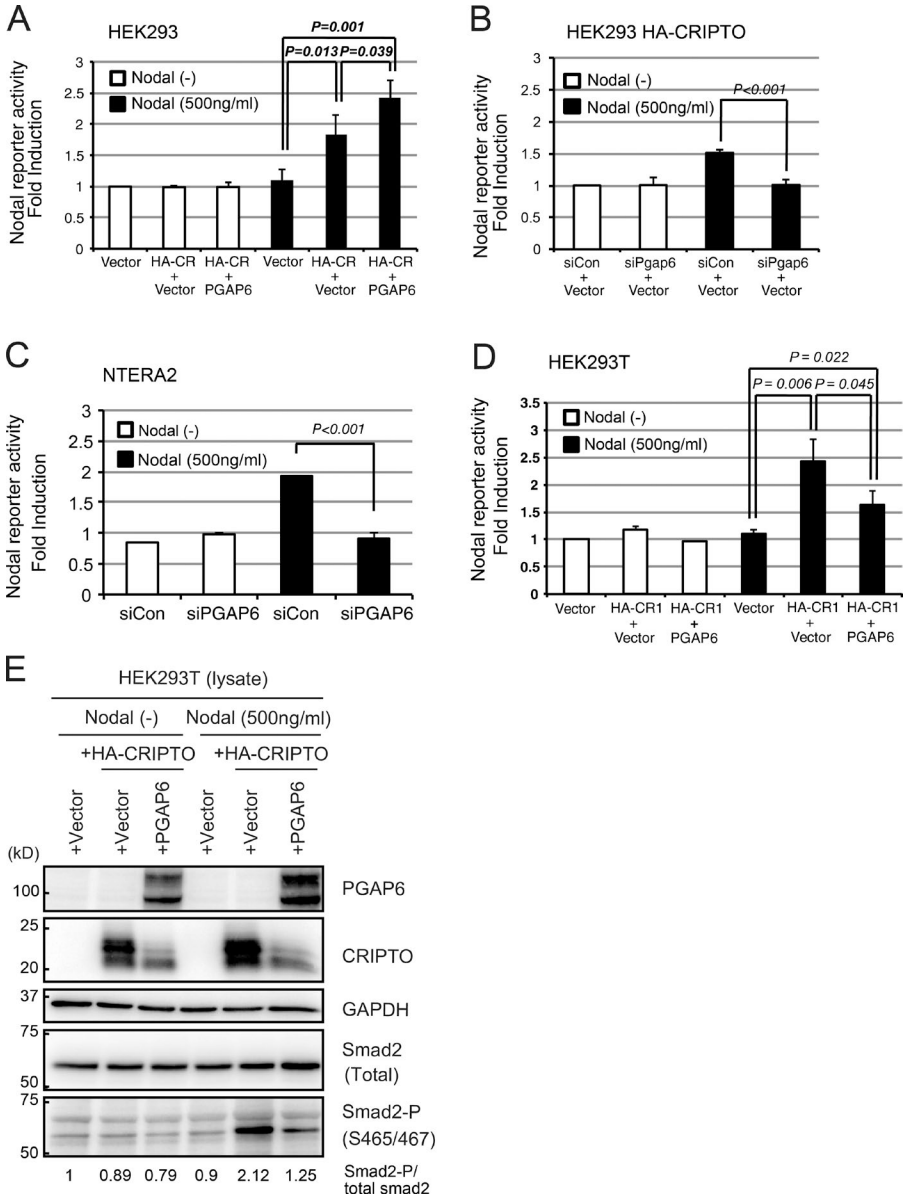

Figure 5. **CRIPTO shed by PGAP6 acts as a Nodal coreceptor in trans.** (A) Nodal coreceptor activity of shed CRIPTO. HEK293 cells transiently expressing HA-CRIPTO with vector or PGAP6 were used as producing cells. HEK293 cells bearing Nodal signal transduction system were used as responder cells. After 6-h culture of the producing cells in serum-free medium, culture supernatants were incubated with responder cells in the presence or absence of Nodal for 12 h. Data shown are the mean ± SD of three independent experiments (Student's *t* test). (B and C) PGAP6-knockdown HEK293 and NTERA2 cells do not shed active CRIPTO. HEK293 cells stably expressing HA-CRIPTO (B) and NTERA2 cells (C) were transfected with control RNA or siRNA against PGAP6 and used as producing cells. Culture supernatants were assayed for CRIPTO activity as described in the legend to A. Data shown are the mean ± SD of three independent experiments (Student's *t* test). (D and E) Cell-associated Nodal signaling by CRIPTO is inhibited by PGAP6. HEK293T cells bearing a Nodal-responsive (n2)7-luc reporter system were transfected with CRIPTO with or without PGAP6. At 24 h after transfection, cells were incubated without or with Nodal for 6 h, and luciferase activities were measured. Data shown in D represent the mean ± SD of three independent experiments (Student's *t* test). The same set of cells was also harvested after 1-h treatment with Nodal and Smad2 phosphorylation was determined (E). Smad2-P to total Smad2 ratios are shown at the bottom of E.

To determine roles of Pgap6 in vivo, we generated and analyzed *Pgap6* KO embryos (Fig. S4). All of the *Pgap6* KO homozygotes except one were embryonic lethal. In wild-type day 6.7 embryos, Cerberus-like (Cerl) was expressed in the anterior visceral endoderm during early gastrulation, and Brachyury, a marker of the primitive streak, was expressed in primitive streak (Belo et al., 1997; Inman and Downs, 2006; Fig. 7 M). In contrast, 3 of 13 *Pgap6* KO embryos at E6.7 showed anterior–posterior axis defect; the Cerl was expressed in distal visceral endoderm, and Brachyury was broadly localized in a proximal area near the embryonic/extraembryonic constriction (Fig. 7 N). These phenotypes, especially impaired anterior shift of Cerl, are common with *Cripto* KO embryos (Ding et al., 1998). In E8.0, growth of *Pgap6* KO embryos was not seen, and their regression was observed. The rest of *Pgap6* KO embryos at E6.7 did not show anterior–posterior axis defect (Fig. 7 O). In E9.0 and E10.0 of most *Pgap6* KO, embryonic development was ceased (Fig. S4). These data strongly suggest that Pgap6 is critical for Cripto function and regulates the anterior–posterior axis formation in embryos.

Discussion

GPI is a cleavable membrane anchor that regulates localization and function of proteins modified with GPI. The major findings of this study were the identifications of PGAP6 as a cell-surface GPI anchor–processing enzyme with GPI-PLA2 activity and of CRIPTO, a GPI-AP required for Nodal signaling, as a sensitive substrate of PGAP6. CRIPTO was processed and released by PGAP6 expressed endogenously in human embryonic carcinoma cell NTERA2. In contrast, CRYPTIC, a GPI-AP that makes the EGF-CFC family with CRIPTO (de Castro et al., 2010), was almost completely resistant to PGAP6 even at overexpressed levels. CD59 and DAF were partially sensitive, and uPAR was nearly completely resistant to overexpressed PGAP6. Therefore, PGAP6 appeared to be a highly selective GPI-PLA2 against CRIPTO. It seems that PGAP6 recognizes not only GPI moiety but also protein structure. We found PGAP6 bearing immature *N*-glycans in the ER. Because a fraction of CRIPTO had immature *N*-glycans suggesting an ER form, it should be rigorously established whether processing of CRIPTO by PGAP6

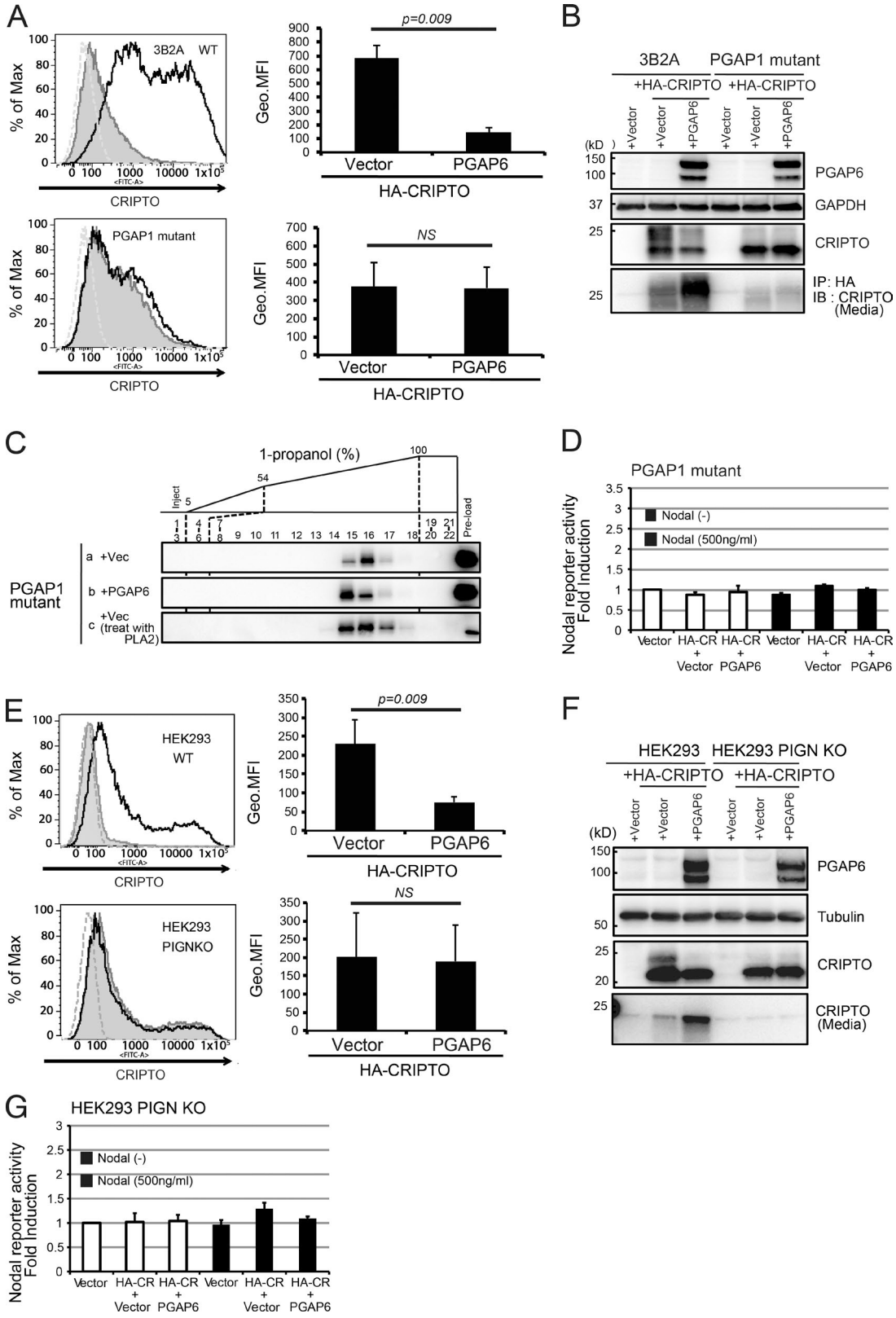

Figure 6. **Mutations in *PGAP1* and *PIGN* inhibited shedding of CRIPTO by PGAP6.** (A and B) CRIPTO was not shed by PGAP6 from *PGAP1* mutant cells. 3B2A or *PGAP1* mutant CHO cells stably expressing HA-CRIPTO were electroporated with vector or PGAP6. The surface expression of HA-CRIPTO was analyzed by flow cytometry (A). Shaded areas, cells carrying vector; black lines, cells carrying PGAP6; dashed lines, cells stained without first IgG. Geometric means of mean fluorescence intensity (Geo.MFI) and SD of three independent experiments are shown on the right (Student's *t* test). The cell lysates and medium samples immunoprecipitated with anti-HA were detected with the indicated antibodies (B). (C) Analysis of GPI-AP lipid structure in *PGAP1* mutant cells. *PGAP1* mutant cells stably expressing vector (a: +Vec) or PGAP6 (b: +PGAP6) were transiently transfected with VSVGts-FF-mEGFP-GPI and analyzed as described in Fig. 3 B. (D) Nodal coreceptor activity is not generated from *PGAP1* mutant cells. *PGAP1* mutant cells transiently transfected with

occurs only at the cell surface or if it could also occur in other locations within the secretory pathway.

We showed that CRIPTO shed by PGAP6 was active as a Nodal coreceptor and that PGAP6-mediated release of CRIPTO reduced Nodal signaling in cells on which CRIPTO was expressed. Furthermore, Pgap6 was involved, similarly to Cripto, in correct formation of the anterior–posterior axis in mouse embryos, indicating that at least one critical function of PGAP6 is to shed CRIPTO. This is a clear example of one of the two biological functions of GPI-AP shedding, namely, shed GPI-AP functions at cells different from the cell on which the GPI-AP was originally expressed.

We used an exon-trap construct to disrupt *Pgap6* in making the *Pgap6*-KO mice. A leakiness of the exon trap seems to be the basis of the variable phenotypes of the *Pgap6*-KO mice, namely, of 244 pups born from crosses of heterozygous mice, 1 was homozygous (Fig. S4), and only 3 of 13 homozygous embryos had abnormal anterior–posterior axis formation (Fig. 7). All of the studied homozygous *Pgap6* KO that passed the stage of anterior–posterior axis formation died before day 9. It seems, therefore, that Pgap6 has roles in other Nodal-dependent processes.

It has been reported that defects in GPI–ethanolamine phosphate transferase I, Pign, and GPI–inositol deacylase Pgap1 perturbed Cripto signaling during forebrain development and caused holoprosencephaly (McKean and Niswander, 2012). We found that the PGAP6-mediated release of CRIPTO was negligible in cells defective in *PGAP1* and *PIGN*. It is possible that the phenotypes of *Pgap1* and *Pign* mutant mice could be caused by inefficient Cripto secretion by Pgap6.

We identified three steps in the generation of hydrophilic CRIPTO from the surface (Fig. 4). First, an acyl-chain at the sn-2 position of GPI in CRIPTO is cleaved by PLA2 activity of PGAP6, generating a lyso-form of CRIPTO (step 1). Lyso-CRIPTO is not stable on the membrane and is shed into the medium (step 2). Shed lyso-CRIPTO is further cleaved by PLD in the medium (step 3). GPI-PLD accounts for a part of the PLD activity acting in step 3. GPI-PLD cannot efficiently cleave GPI-APs associated with the membrane and requires detergents for efficient cleavage (Low and Huang, 1991). However, if GPI anchors become lyso-forms, they could be cleaved more efficiently. It is possible that cleavage of a lyso-form of CRIPTO by GPI-PLD might occur even before release of the lyso-form from the PM. Because many GPI-APs form transient homodimers (Suzuki et al., 2012; Seong et al., 2013), CRIPTO might also form homodimers transiently. A homodimer of lyso–GPI-CRIPTO has two acyl chains and would be stably associated with the membrane. However, a reported $t_{1/2}$ of transient homodimers of GPI-APs is short (in a range of 100–200 ms), and a release from the membrane is expected to occur during the monomeric state. It was also reported that shedding of CRIPTO was mediated by GPI-PLD activity (Watanabe et al., 2007). CRIPTO is constantly released into the medium in the presence of 10% serum, and serum growth factors induce the release of CRIPTO via activation of PLCγ and PKC signaling. Thus, PGAP6 might be the target of regulation. Indeed, shedding of CRIPTO was inhibited by PGAP6 knockdown even in the presence of 10% serum. The regulation of PGAP6 activity needs to be addressed to better understand the spatiotemporal regulation of CRIPTO functions.

Materials and methods

Cells, antibodies, and materials

HEK293T HA-CRIPTO stably expressing HA-tagged CRIPTO was established by transfection of linearized pME-pgkpuro-HA-CR1 and cultured in DMEM containing 10% FCS and 10 µg/ml puromycin. To prepare pME-pgkpuro-HA-CR1, we obtained human CRIPTO cDNA (Kazusa DNA Res. Inst.) and cloned it into a mammalian expression plasmid pME bearing a puromycin resistance gene and a segment of signal sequence plus HA tag (Table S1). 3B2A cells are derived from CHO-K1 cells and stably express two human GPI-APs, CD59 and DAF (Nakamura et al., 1997). All CHO cell lines, including 3B2A wild-type and 3B2A cells stably expressing HFGF-CD59, HA-TMEM8A, HF-TMEM8A, TMEM8A-Flag, or HA-CRYPTIC (human CRYPTIC HA-tagged at the N terminus after the ER signal sequence), were cultured in Ham's F-12 medium containing 10% FCS with 6 µg/ml blasticidin, 10 µg/ml puromycin, or 500 µg/ml hygromycin, if necessary. Human CRYPTIC cDNA (clone AK315326) was obtained from NITE Biological Resource Center. NTERA2 cells (clone D1) were obtained from ATCC and cultured in DMEM containing 10% FCS. *PIGN* and *GPLD1* genes were disrupted by the CRISPR-Cas9 gene editing system (Cong et al., 2013) to generate HEK293-PIGN-KO (Ohba et al., 2014) and HEK293-GPLD-KO cells, respectively. Antibodies used were monoclonal rabbit anti–CRIPTO, polyclonal rabbit anti–Na/K ATPase 1, anti-Smad2, and anti–phospho-Smad2 S465/467 (Cell Signaling Technology); anti-GPP130 (Covance); monoclonal mouse anti–Flag (M2) and anti–HA-tag (H7; Sigma-Aldrich); anti-GAPDH (Ambion); anti-tubulin and anti-transferrin receptor (Invitrogen); anti–caveolin-1 and anti–syntaxin 6 (BD); anti–ribophorin I (Santa Cruz Biotechnology, Inc.); and anti-DAF (1A10), anti-CD59 (5H8), and anti-uPAR (5D6; Maeda et al., 2007). Mouse anti–human TMEM8A mAb (clone 5C3; IgG2b) was a gift from BioLegend. Polyclonal rabbit anti–PGAP6 was raised by immunization with a peptide corresponding to the C-terminal cytosolic tail of mouse PGAP6 (SCRUM Inc.). Secondary antibodies used were HRP-conjugated anti–mouse IgG (GE Healthcare); anti–rabbit IgG (Cell Signaling Technology); phycoerythrin-conjugated goat anti–mouse IgG (BD); Alexa Fluor 488–conjugated goat anti–mouse IgG, goat anti–rabbit IgG, and Alexa Fluor 594–conjugated goat anti–rabbit IgG (Thermo Fisher Scientific).

Immunoprecipitation of secreted HA-CRIPTO

3B2A cells (5×10^6) were electroporated with 12 µg pME-HA-CRIPTO plasmid at 250 V and 1,000 µF using a Gene Pulser (Bio-Rad Laboratories). For HEK293T cells (2×10^5), plasmids were transfected using Lipofectamine 2000 (Invitrogen) and incubated for 24 h. At 24 or 52 h after transfection, cells were incubated with serum-free medium for 6 h. The culture medium was collected, and anti-HA beads (clone

HA-CRIPTO and vector or PGAP6 were cultured, and CRIPTO activities in the culture supernatants were assayed as described in Fig. 5 A. Data shown represent the mean ± SD of three independent experiments. (E and F) CRIPTO was not released from *PIGN* mutant cells by PGAP6. HEK293 or *PIGN*-KO cells were transfected with HA-CRIPTO and vector or PGAP6. The surface expression of HA-CRIPTO was analyzed by flow cytometry (E). Lines are indicated as in A. Geo.MFI and SD of three independent experiments are shown on the right (Student's *t* test). The cell lysates and medium samples immunoprecipitated with anti-HA beads were analyzed by Western blotting (F). (G) Nodal coreceptor activity is not generated from *PIGN*-KO cells. *PIGN*-KO HEK293 cells transfected with HA-CRIPTO and vector or PGAP6 were cultured, and CRIPTO activities were assayed as described in Fig. 5 A. Data shown represent the mean ± SD of three independent experiments.

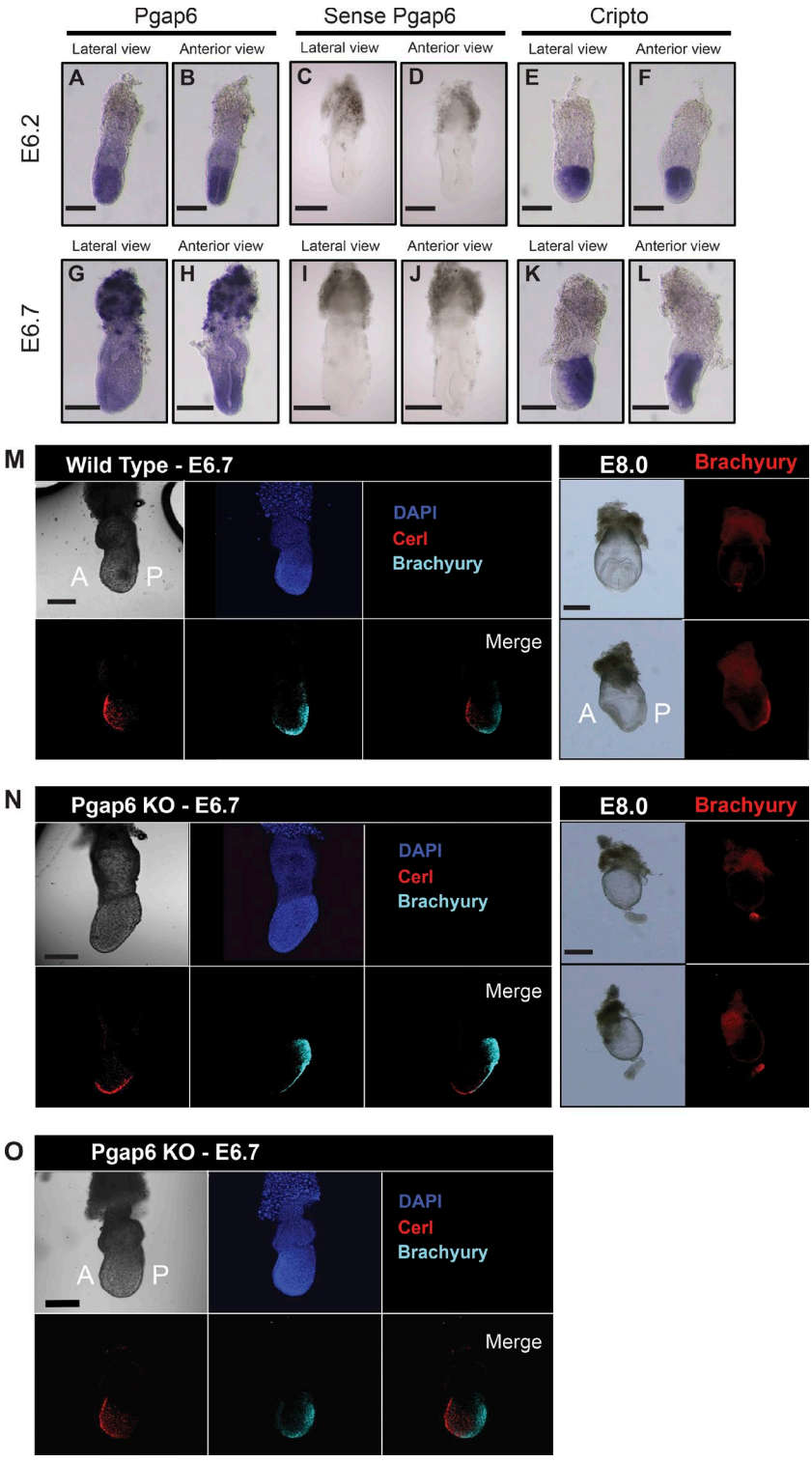

Figure 7. **Pgap6 is required for anterior–posterior axis formation in embryos.** (A–L) In situ hybridization of *Pgap6* and *Cripto* in mouse embryos. Epiblasts in E6.2 (A–F) and E6.7 (G–L) mouse embryos expressed *Pgap6* (A, B, G, and H) and *Cripto* (E, F, K, and L). (C, D, I, and J) Pgap6 sense controls. Bars, 0.5 mm. Immunofluorescence analysis of embryo markers in wild-type (M) and *Pgap6* KO (N, with phenotype; O, without phenotype) mice. Whole embryos of E6.7 and E8.0 were subjected to immunofluorescence analysis with antibodies to Cerl (red in E6.7 embryos) and Brachyury (cyan in E6.7 embryos or red in E8.0 embryos). A, anterior; P, posterior. Bars: (E6.7) 0.5 mm; (E8.0) 1 mm.

H7) were added and incubated with rotation for 1 h at 4°C. Beads were washed four times with PBS. Immunoprecipitated proteins were eluted using 4× SDS-PAGE sample buffer and boiled for 5 min. Samples were subjected to SDS-PAGE, and proteins were probed by Western blotting.

Triton X-114 partitioning

Triton X-114 partitioning of GPI-APs was performed as described previously with some modification (Doering et al., 2001). Cells (10^6) were lysed in lysis buffer (20 mM Tris-HCl, pH 7.4, 150 mM NaCl, 5 mM EDTA, complete protease inhibitors [Roche], and 2% Triton X-114) for 30 min on ice. Supernatants were collected to new tubes and proteins precipitated by cold acetone (eight times volume) after incubation for 1 h at −80°C. After centrifugation, the precipitated proteins were solubilized in lysis buffer, and phase separation was performed by warming up to 37°C and subsequent centrifugation at 37°C and 1,000 *g* for 10 min. The upper aqueous phase and lower detergent phase were collected and subjected to SDS-PAGE followed by Western blotting to determine partitioned proteins.

FACS analysis

HEK293T and 3B2A cells (5×10^6) transfected with plasmids and NTERA2 cells were harvested with PBS containing 5 mM EDTA and 0.1% BSA. After washing with FACS buffer (PBS containing 1% BSA and 0.1% sodium azide), cells were incubated for 25 min with anti-CRIPTO, anti-TMEM8A, anti-DAF, anti-CD59, or anti-HA antibodies (20 µg/ml) on ice. In some cases, cells were treated with phosphatidylinositol-specific PLC (PI-PLC) before staining by antibodies. For this, four volumes of cells (1.25×10^7/ml in F12 medium without FCS) were mixed with one volume of 5 U/ml PI-PLC (from *Bacillus cereus*; Invitrogen) in PBS supplemented with 0.5% BSA, 5 mM EDTA, and 10 mM Hepes and incubated for 1 h at 37°C. After incubation with antibodies, cells were washed with FACS buffer three times. Cells were incubated for 25 min with anti–rabbit Alexa Fluor 488–conjugated antibody or anti–mouse IgG phycoerythrin-conjugated antibody (1:100) on ice. Cells were then pelleted, suspended in 300 µl FACS buffer, and analyzed using an FACS Canto II (BD).

Subcellular fractionation

Cells were washed twice with buffer (0.25 M sucrose in 20 mM Hepes-NaOH, pH 7.4), homogenized three times at 4°C in the same buffer using a tight-fitting Dounce pestle, and debris removed by centrifugation at 3,310 *g* for 10 min. The supernatant was placed on a 2-M sucrose cushion and ultracentrifuged at 200,000 *g* for 1 h. The pellet was resuspended and sucrose concentration was adjusted to 1.5 M. A discontinuous sucrose gradient was generated in an SW41 tube (Beckman Coulter) by overlaying the following sucrose solutions all in buffer consisting of 150 mM NaCl and 20 mM Hepes-NaOH, pH 7.4: 1.5 ml of 2 M, 2 ml of 1.7 M, 3 ml supernatant, 2 ml of 1.25 M, 2 ml of 0.9 M, and 1.5 ml of 0.5 M. The gradient was centrifuged at 110,000 *g* in an SW41 rotor (Beckman Coulter) for 2 h. Fractions were collected from the top. Equal aliquots of fractions were subjected to SDS-PAGE and proteins probed by Western blotting. Organelles in each fraction were identified by determining the PM marker Na/K ATPase 1, ER marker ribophorin I, and Golgi marker syntaxin 6. The His-Flag–tagged PGAP6 was determined by anti-PGAP6 and anti-Flag antibodies.

Fractionation of GPI-APs with Octyl-FF column

3B2A cells stably transfected with vector or PGAP6 (2×10^7) were electroporated with pME-Neo-VSVGts-FF-mEGFP-GPI (Tashima et al., 2006). Cells were cultured for 12 h at 37°C followed by 1.5 d at 32°C and harvested using PBS containing 2.5 mM EDTA and 0.5% BSA. After centrifugation, the cell pellet was suspended in 2.5 ml buffer (20 mM Tris-HCl, pH 7.4, 150 mM NaCl, and 1 mM EDTA) and incubated for 1 h on ice. The supernatants were collected and incubated with anti-Flag (M2) beads overnight. Beads were washed two times with 0.5 ml wash buffer 1 (30 mM 1-octyl-β-D-glucoside, 20 mM Tris-HCl, pH 7.4, 150 mM NaCl, and 1 mM EDTA), two times with 0.5 ml wash buffer 2 (20 mM Tris-HCl, pH 7.4, and 0.1% NP-40), and two times with 0.5 ml wash buffer 3 (20 mM Tris-HCl, pH 7.4, and 0.03% NP-40). Flag-mEGFP-GPI was eluted three times with 150 µl elution buffer (0.1 M ammonium acetate containing 1 mg/ml Flag-peptide [Sigma-Aldrich] and 0.03% NP-40). For PLA2 treatment, immunoprecipitates bound to anti-Flag beads were washed, suspended in buffer (100 mM Tris-HCl, pH 7.4, 6 mM $CaCl_2$, and 0.1% NP-40), and treated with 75 U honeybee PLA2 (Sigma-Aldrich) at 37°C for 6 h. The beads were washed with wash buffers 2 and 3 and eluted as in a similar way. A 100-µl aliquot of the eluate was mixed with 100 µl buffer (0.1 M ammonium acetate, 0.03% NP-40, and 10% 1-propanol), loaded onto an Octyl-FF column (GE Healthcare), and chromatographed in ÄKTA (GE Healthcare) at a flow rate of 0.5 ml/min using a 54–100% gradient of 1-propanol. Fractions were collected, dried, subjected to SDS-PAGE, and proteins were probed by Western blotting using an anti-Flag (M2) antibody.

Immunofluorescence microscopy

3B2A cells (5×10^6) electroporated with HF-PGAP6 together with Lyn11-mRFP or RFP-KDEL constructs were cultured for 2 d and fixed with 4% PFA in PBS for 25 min at room temperature. After quenching with 40 mM ammonium chloride in PBS, the cells were permeabilized with or without PBS containing 0.1% Triton X-100 for 1 h at room temperature. The cells were stained with mouse anti–TMEM8A or anti–Flag with or without rabbit anti–GPP130 followed by Alexa Fluor 488–conjugated goat anti–mouse IgG with or without Alexa Fluor 594–conjugated goat anti–rabbit IgG antibodies. Confocal images were acquired on a FluoView FV1000 (Olympus).

Dual luciferase assay

HEK293T cells (8×10^4) were transfected with HA-tagged CRIPTO either with an empty vector or PGAP6 plasmid, plus Nodal-responsive luciferase reporter construct (Saijoh et al., 2000), FAST2, ALK4, and pTK-Renilla using FuGene transfection reagent (Promega). At 24 h after transfection, medium was replaced with serum-free medium with or without 500 ng/ml recombinant human Nodal (R&D Systems) and incubated for 6 h. Luciferase activity was measured using a dual luciferase reporter assay kit (Promega). These experiments were repeated three times independently with triplicate samples.

Liquid chromatography/electrospray ionization–tandem mass spectrometry analysis

We generated 3B2A cells stably expressing CD59 with tandem His, Flag, GST, and Flag-tags at the N terminus after the signal sequence (HFGF-CD59; Tashima et al., 2006). The cells were stably transfected with an empty vector or PGAP6 and selected in 1 µg/ml puromycin. Expressed and released HFGF-CD59 was purified from the culture medium by glutathione Sepharose 4B and eluted with a solution (20 mM reduced glutathione, 30 mM Tris-HCl, pH 8.0, and 150 mM NaCl). Purified HFGF-CD59 was subjected to SDS-PAGE, stained with Imperial CBB (Thermo Fisher Scientific), and digested by trypsin. The extracted peptides from the SDS-PAGE gel were directly analyzed by liquid chromatography–tandem MS (LC-MS/MS) using an L-column (C18, 0.1 × 150 mm; Chemicals Evaluation and Research Institute) on a nanoflow LC system (Advance UHPLC; Bruker) coupled to a mass spectrometer (TQ Orbitrap Velos; Thermo Fisher Scientific). The mass spectrometer was operated in the positive ion mode with data-dependent MS/MS. Details were described previously (Tashima et al., 2006; Fujita et al., 2009).

Knockdown of PGAP6 by siRNA

HEK293T and NTERA2 cells (2×10^6 cells) were transfected with siPGAP6 (sense, 5′-CCUCCAUGAUGACUAGCGATT-3′; and antisense, 5′-UCGCUAGUCAUCAUGGAGGTG-3′; Ambion) or siControl by RNAi MAX reagent (Invitrogen) on day 0 with 30 pmol siRNA and on day 1 with 60 pmol siRNA. On day 3, cells were assessed for knockdown efficiency by either quantitative PCR or flow cytometry and for phenotypic changes.

Whole-mount in situ hybridization

Embryos were carefully staged based on their morphology. They were fixed overnight at 4°C in PBS containing 4% PFA, washed twice with PBS, and dehydrated with methanol series. Whole-mount in situ hybridization was performed using standard procedures (Wilkinson, 1992) with digoxigenin-labeled riboprobes specific for *Cripto* (Ding et al., 1998; Xu et al., 1999) and *Pgap6*. The full-length antisense and sense

riboprobes for *Pgap6* were synthesized from FANTOM2 cDNA clone (AK044384; 2.6 kb). E6.2 and E6.7 embryos were from the ICR strain.

Generation of Pgap6 KO mice

To generate *Pgap6/Tmem8a* (Mouse Genome Informatics identification number 1926283) KO mice, a targeting construct was obtained from European Conditional Mouse Mutagenesis. The construct was electroporated into EGR-G101 embryonic stem (ES) cells (Fujihara et al., 2013a), followed by selection. The ES cells with the construct correctly targeted into the *Pgap6* genomic locus were injected into blastocysts, and chimeric males were obtained. Using the chimeric male mice and C57BL/6 female mice, heterozygous KO mice were generated. Genotyping was performed with a mixture of three PCR primers (Fig. S4). The *Pgap6* heterozygous KO strains were maintained in a C57BL/6 genetic background. All animal experiments were performed according to the guidelines for the Care and Use of Laboratory Animals of Osaka University.

Immunofluorescence analysis of mouse embryos

Embryos were recovered in PBS and carefully staged based on their morphology and cell numbers. They were fixed overnight at 4°C in PBS containing 4% PFA, washed twice with PBS, permeabilized with 0.2% Triton X-100 in PBS for 30 min at room temperature, incubated for 1 h at room temperature with TSA blocking reagent (PerkinElmer), and incubated overnight at 4°C with the following primary antibodies diluted in blocking reagent. First immunoreaction was performed with goat antibodies to Brachyury (1/50 dilution; N-19, #sc-17743; Santa Cruz Biotechnology, Inc.) and rat antibodies to Cerl1 (1/100 dilution; MAB1986; R&D Systems). After washing three times with PBS, they were incubated with the following secondary antibodies diluted in TSA blocking reagent. Second antibodies were Alexa Fluor 488 donkey anti–mouse IgG (1/200 dilution; A21206; Molecular Probes), Alexa Fluor 594 donkey anti–rat IgG (1/200 dilution; A21209; Molecular Probes), Alexa Fluor 594 donkey anti–goat IgG (1/200 dilution; A11057; Molecular Probes), and Alexa Fluor 633 donkey anti–goat IgG (1/200 dilution; A21082; Molecular Probes). Nuclei were stained by incubation for 30 min with DAPI (1/2,000 dilution in PBS; FQ023; Wako Pure Chemical Industries). Images were obtained with a laser-scanning confocal microscope system (FV1000; Olympus) and a UPLSAPO 20× (NA 0.75; Olympus) objective lens. Embryos were genotyped by PCR analysis with their parts.

Online supplemental material

Fig. S1 shows that *PGAP6* knockdown inhibits release of mature CRIPTO from the cell surface even in the presence of serum. Fig. S2 shows functional analysis of PGAP6 point mutants demonstrating that amino acids conserved in the CREST superfamily are functionally important, except S584A. Fig. S3 shows LC/electrospray ionization (ESI)-MS/MS analysis of GPI moiety in HFGF-CD59 shed by PGAP6. Fig. S4 shows the procedure and some characteristics of *Pgap6* KO mice. Table S1 contains primers used in this study.

Acknowledgments

The authors thank Drs. Ryo Taguchi, Hidetaka Shiratori, and Tatsuo Michiue for helpful discussion; BioLegend (Osaka, Japan) for anti-TMEM8A mAb; and Keiko Kinoshita, Kana Miyanagi, and Yukari Hirata for technical help.

This work was supported by grants-in-aid from the Japan Society for the Promotion of Science (to T. Kinoshita and M. Fujita), the Takeda Science Foundation, the National Science Foundation for Young Scientists of China (grant 31400693), the Natural Science Foundation of Jiangsu Province (grant BK20140141), and Research Funds for the Central Universities (grant JUSRP11540 to M. Fujita).

The authors declare no competing financial interests.

Author contributions: G.-H. Lee performed the main experiments and wrote an original draft; M. Fujita proposed the project, performed initial experiments, and wrote a paper; K. Takaoka, E. Kajikawa, and H. Hamada analyzed mouse embryos; Y. Murakami analyzed KO mice; Y. Fujihara and M. Ikawa generated and analyzed KO mice; N. Kanzawa, Y. Takada, and K. Saito determined GPI structure by MS analysis; K. Murakami generated GPI-PLD KO cells and performed experiments with them; Y. Maeda designed cell biological experiments and edited a paper; and T. Kinoshita supervised the project and wrote a paper.

Submitted: 31 May 2016
Revised: 24 August 2016
Accepted: 2 November 2016

References

Belo, J.A., T. Bouwmeester, L. Leyns, N. Kertesz, M. Gallo, M. Follettie, and E.M. De Robertis. 1997. Cerberus-like is a secreted factor with neutralizing activity expressed in the anterior primitive endoderm of the mouse gastrula. *Mech. Dev.* 68:45–57. http://dx.doi.org/10.1016/S0925-4773(97)00125-1

Chu, J., J. Ding, K. Jeays-Ward, S.M. Price, M. Placzek, and M.M. Shen. 2005. Non-cell-autonomous role for Cripto in axial midline formation during vertebrate embryogenesis. *Development.* 132:5539–5551. http://dx.doi.org/10.1242/dev.02157

Cong, L., F.A. Ran, D. Cox, S. Lin, R. Barretto, N. Habib, P.D. Hsu, X. Wu, W. Jiang, L.A. Marraffini, and F. Zhang. 2013. Multiplex genome engineering using CRISPR/Cas systems. *Science.* 339:819–823. http://dx.doi.org/10.1126/science.1231143

de Castro, N.P., M.C. Rangel, T. Nagaoka, D.S. Salomon, and C. Bianco. 2010. Cripto-1: An embryonic gene that promotes tumorigenesis. *Future Oncol.* 6:1127–1142. http://dx.doi.org/10.2217/fon.10.68

Ding, J., L. Yang, Y.T. Yan, A. Chen, N. Desai, A. Wynshaw-Boris, and M.M. Shen. 1998. Cripto is required for correct orientation of the anterior-posterior axis in the mouse embryo. *Nature.* 395:702–707. http://dx.doi.org/10.1038/27215

Doering, T.L., P.T. Englund, and G.W. Hart. 2001. Detection of glycophospholipid anchors on proteins. Curr. Protoc. Protein Sci. Chapter 12:Unit 12 15.

Ferguson, M.A.J., T. Kinoshita, and G.W. Hart. 2009. Glycosylphosphatidylinositol anchors. In Essentials of Glycobiology. Second edition. A. Varki, R.D. Cummings, J.D. Esko, H.H. Freeze, P. Stanley, C.R. Bertozzi, G.W. Hart, and M.E. Etzler, editors. Cold Spring Harbor Laboratory Press, Cold Spring Harbor, NY. 143–161.

Fujihara, Y., and M. Ikawa. 2016. GPI-AP release in cellular, developmental, and reproductive biology. *J. Lipid Res.* 57:538–545. http://dx.doi.org/10.1194/jlr.R063032

Fujihara, Y., K. Kaseda, N. Inoue, M. Ikawa, and M. Okabe. 2013a. Production of mouse pups from germline transmission-failed knockout chimeras. *Transgenic Res.* 22:195–200. http://dx.doi.org/10.1007/s11248-012-9635-x

Fujihara, Y., K. Tokuhiro, Y. Muro, G. Kondoh, Y. Araki, M. Ikawa, and M. Okabe. 2013b. Expression of TEX101, regulated by ACE, is essential for the production of fertile mouse spermatozoa. *Proc. Natl. Acad. Sci. USA.* 110:8111–8116. http://dx.doi.org/10.1073/pnas.1222166110

Fujita, M., M. Umemura, T. Yoko-o, and Y. Jigami. 2006. PER1 is required for GPI-phospholipase A2 activity and involved in lipid remodeling of GPI-anchored proteins. *Mol. Biol. Cell.* 17:5253–5264. http://dx.doi.org/10.1091/mbc.E06-08-0715

Fujita, M., Y. Maeda, M. Ra, Y. Yamaguchi, R. Taguchi, and T. Kinoshita. 2009. GPI glycan remodeling by PGAP5 regulates transport of GPI-anchored proteins from the ER to the Golgi. *Cell.* 139:352–365. http://dx.doi.org/10.1016/j.cell.2009.08.040

Hong, Y., Y. Maeda, R. Watanabe, K. Ohishi, M. Mishkind, H. Riezman, and T. Kinoshita. 1999. Pig-n, a mammalian homologue of yeast Mcd4p, is

involved in transferring phosphoethanolamine to the first mannose of the glycosylphosphatidylinositol. *J. Biol. Chem.* 274:35099–35106. http://dx.doi.org/10.1074/jbc.274.49.35099

Inman, K.E., and K.M. Downs. 2006. Localization of Brachyury (T) in embryonic and extraembryonic tissues during mouse gastrulation. *Gene Expr. Patterns.* 6:783–793. http://dx.doi.org/10.1016/j.modgep.2006.01.010

Kondoh, G., H. Tojo, Y. Nakatani, N. Komazawa, C. Murata, K. Yamagata, Y. Maeda, T. Kinoshita, M. Okabe, R. Taguchi, and J. Takeda. 2005. Angiotensin-converting enzyme is a GPI-anchored protein releasing factor crucial for fertilization. *Nat. Med.* 11:160–166. http://dx.doi.org/10.1038/nm1179

Low, M.G., and K.S. Huang. 1991. Factors affecting the ability of glycosylphosphatidylinositol-specific phospholipase D to degrade the membrane anchors of cell surface proteins. *Biochem. J.* 279:483–493. http://dx.doi.org/10.1042/bj2790483

Maeda, Y., Y. Tashima, T. Houjou, M. Fujita, T. Yoko-o, Y. Jigami, R. Taguchi, and T. Kinoshita. 2007. Fatty acid remodeling of GPI-anchored proteins is required for their raft association. *Mol. Biol. Cell.* 18:1497–1506. http://dx.doi.org/10.1091/mbc.E06-10-0885

McKean, D.M., and L. Niswander. 2012. Defects in GPI biosynthesis perturb Cripto signaling during forebrain development in two new mouse models of holoprosencephaly. *Biol. Open.* 1:874–883. http://dx.doi.org/10.1242/bio.20121982

Minchiotti, G., S. Parisi, G. Liguori, M. Signore, G. Lania, E.D. Adamson, C.T. Lago, and M.G. Persico. 2000. Membrane-anchorage of Cripto protein by glycosylphosphatidylinositol and its distribution during early mouse development. *Mech. Dev.* 90:133–142. http://dx.doi.org/10.1016/S0925-4773(99)00235-X

Minchiotti, G., G. Manco, S. Parisi, C.T. Lago, F. Rosa, and M.G. Persico. 2001. Structure-function analysis of the EGF-CFC family member Cripto identifies residues essential for nodal signalling. *Development.* 128:4501–4510.

Nakamura, N., N. Inoue, R. Watanabe, M. Takahashi, J. Takeda, V.L. Stevens, and T. Kinoshita. 1997. Expression cloning of PIG-L, a candidate N-acetylglucosaminyl-phosphatidylinositol deacetylase. *J. Biol. Chem.* 272:15834–15840. http://dx.doi.org/10.1074/jbc.272.25.15834

Ohba, C., N. Okamoto, Y. Murakami, Y. Suzuki, Y. Tsurusaki, M. Nakashima, N. Miyake, F. Tanaka, T. Kinoshita, N. Matsumoto, and H. Saitsu. 2014. PIGN mutations cause congenital anomalies, developmental delay, hypotonia, epilepsy, and progressive cerebellar atrophy. *Neurogenetics.* 15:85–92. (published erratum appears in *Neurogenetics*. 2014. 15:93) http://dx.doi.org/10.1007/s10048-013-0384-7

Parisi, S., D. D'Andrea, C.T. Lago, E.D. Adamson, M.G. Persico, and G. Minchiotti. 2003. Nodal-dependent Cripto signaling promotes cardiomyogenesis and redirects the neural fate of embryonic stem cells. *J. Cell Biol.* 163:303–314. http://dx.doi.org/10.1083/jcb.200303010

Park, S., C. Lee, P. Sabharwal, M. Zhang, C.L. Meyers, and S. Sockanathan. 2013. GDE2 promotes neurogenesis by glycosylphosphatidylinositol-anchor cleavage of RECK. *Science.* 339:324–328. http://dx.doi.org/10.1126/science.1231921

Paulick, M.G., and C.R. Bertozzi. 2008. The glycosylphosphatidylinositol anchor: A complex membrane-anchoring structure for proteins. *Biochemistry.* 47:6991–7000. http://dx.doi.org/10.1021/bi8006324

Pei, J., D.P. Millay, E.N. Olson, and N.V. Grishin. 2011. CREST--a large and diverse superfamily of putative transmembrane hydrolases. *Biol. Direct.* 6:37. http://dx.doi.org/10.1186/1745-6150-6-37

Saijoh, Y., H. Adachi, R. Sakuma, C.Y. Yeo, K. Yashiro, M. Watanabe, H. Hashiguchi, K. Mochida, S. Ohishi, M. Kawabata, et al. 2000. Left-right asymmetric expression of lefty2 and nodal is induced by a signaling pathway that includes the transcription factor FAST2. *Mol. Cell.* 5:35–47. http://dx.doi.org/10.1016/S1097-2765(00)80401-3

Seong, J., Y. Wang, T. Kinoshita, and Y. Maeda. 2013. Implications of lipid moiety in oligomerization and immunoreactivities of GPI-anchored proteins. *J. Lipid Res.* 54:1077–1091. http://dx.doi.org/10.1194/jlr.M034421

Shen, M.M. 2007. Nodal signaling: developmental roles and regulation. *Development.* 134:1023–1034. http://dx.doi.org/10.1242/dev.000166

Shen, M.M., and A.F. Schier. 2000. The EGF-CFC gene family in vertebrate development. *Trends Genet.* 16:303–309. http://dx.doi.org/10.1016/S0168-9525(00)02006-0

Suzuki, K.G., R.S. Kasai, K.M. Hirosawa, Y.L. Nemoto, M. Ishibashi, Y. Miwa, T.K. Fujiwara, and A. Kusumi. 2012. Transient GPI-anchored protein homodimers are units for raft organization and function. *Nat. Chem. Biol.* 8:774–783. http://dx.doi.org/10.1038/nchembio.1028

Tanaka, S., Y. Maeda, Y. Tashima, and T. Kinoshita. 2004. Inositol deacylation of glycosylphosphatidylinositol-anchored proteins is mediated by mammalian PGAP1 and yeast Bst1p. *J. Biol. Chem.* 279:14256–14263. http://dx.doi.org/10.1074/jbc.M313755200

Tashima, Y., R. Taguchi, C. Murata, H. Ashida, T. Kinoshita, and Y. Maeda. 2006. PGAP2 is essential for correct processing and stable expression of GPI-anchored proteins. *Mol. Biol. Cell.* 17:1410–1420. http://dx.doi.org/10.1091/mbc.E05-11-1005

Tian, T., and A.M. Meng. 2006. Nodal signals pattern vertebrate embryos. *Cell. Mol. Life Sci.* 63:672–685. http://dx.doi.org/10.1007/s00018-005-5503-7

Watanabe, K., C. Bianco, L. Strizzi, S. Hamada, M. Mancino, V. Bailly, W. Mo, D. Wen, K. Miatkowski, M. Gonzales, et al. 2007. Growth factor induction of Cripto-1 shedding by glycosylphosphatidylinositol-phospholipase D and enhancement of endothelial cell migration. *J. Biol. Chem.* 282:31643–31655. http://dx.doi.org/10.1074/jbc.M702713200

Wilkinson, D.G. 1992. Whole mount in situ hybridization of vertebrate embryos. In *In Situ* Hybridization: A Practical Approach. Second edition. Oxford University Press, Oxford, UK. 75–83.

Xu, C., G. Liguori, M.G. Persico, and E.D. Adamson. 1999. Abrogation of the Cripto gene in mouse leads to failure of postgastrulation morphogenesis and lack of differentiation of cardiomyocytes. *Development.* 126:483–494.

Yan, Y.T., J.J. Liu, Y. Luo, C. E, R.S. Haltiwanger, C. Abate-Shen, and M.M. Shen. 2002. Dual roles of Cripto as a ligand and coreceptor in the nodal signaling pathway. *Mol. Cell. Biol.* 22:4439–4449. http://dx.doi.org/10.1128/MCB.22.13.4439-4449.2002